Nanometer Scale Surface Properties of Supported Lipid Bilayers Measured with Hydrophobic and Hydrophilic Atomic Force Microscope Probes †

ARTICLE *in* LANGMUIR · MARCH 2003

Impact Factor: 4.46 · DOI: 10.1021/la026382z

Nanometer Scale Surface Properties of Supported Lipid Bilayers Measured with Hydrophobic and Hydrophilic Atomic Force Microscope Probes†

James Schneider,‡ William Barger, and Gil U. Lee*,§

Chemistry Division, Code 6170, Naval Research Laboratory, Washington, D.C. 20375-5342

Received August 9, 2002

Using the atomic force microscope (AFM), surface-forces measurements are made in water between chemically modified AFM probes and model membranes created by Langmuir−Blodgett (LB) deposition. A series of four different lipid monolayers with varying headgroups and monolayer properties were transferred onto monolayers on mica for analysis. Using a hydrophilic probe, the bilayers are elastically deformed at low load and punctured at a repeatable, material-dependent breakthrough force. Using hydrophobic probes, the bilayers are punctured on contact, at loads near zero, in all cases. This effect is also manifest when imaging mixed LB monolayers, which show a large topography contrast at low load when using hydrophilic tips but none when using hydrophobic tips. These results provide evidence that the forces required to deform lipid bilayers are dramatically changed in the vicinity of nonpolar surfaces, which is central to the understanding of membrane fusion processes and the function of membrane-associated proteins.

Introduction

Of central importance to the barrier function of biological membranes is their ability to selectively resist and encourage strong membrane−membrane adhesion and fusion. In addition to electrostatic forces, several strong repulsions which become significant at separations of 3 nm or less have been identified which act to prevent the coalescence of lipid membranes.[1−3] These include a "hydration force"[1] required to remove waters of hydration from lipid headgroups, entropically derived steric forces arising from the suppression of membrane fluctuational modes on their mutual approach ("undulation forces", "peristaltic forces", and "protrusion forces"),[2] and mechanical forces arising from the rearrangement of overlapping lipid headgroups and the eventual deformation of the membrane lipids themselves. Potentially, all these contributions to the membrane−membrane interaction free energy have a similar strength and range of operation, which has greatly complicated assigning their significance in particular systems.[2] Often, the collective action of these short-range repulsions has been called a "steric/hydration force" to reflect this ambiguity.

Of course, for proper cell function membrane−membrane fusion must be induced under some conditions. Fusion has been induced in model bilayer systems by mechanically stressing the bilayers, creating an osmotic gradient across them, or by adding certain fusogenic agents.[4,5] Exposure of the lipid membrane to hydrophobic surfaces is a key event in each case. It is believed that mechanical, thermal, or osmotic stressing of bilayers exposes the hydrophobic interior of the bilayers somewhat to interact with approaching bilayers. The fusogenic capacity of calcium has been traced to its ability to induce phase separation in model membranes, exposing hydrophobic surface at phase boundaries.[6] Fusion proteins, such as those employed by viruses, aggregate in the vicinity of membranes and generally have significant hydrophobic segments.[5]

Because the steric/hydration barriers to membrane fusion are so formidable, it has been proposed that nonmembrane intermediates are formed prior to the fusion event, so that weakly repulsive or even attractive forces are felt between these intermediates and the repulsive forces are bypassed.[7] The "stalk" hypothesis contends that the random exposure of hydrophobic segments is a precursor to fusion.[8] The formation of membrane pores prior to membrane fusion has been extensively documented in living systems.[9] Certain "nonbilayer lipids" with high degrees of spontaneous curvature can facilitate membrane fusion by helping to stabilize these intermediates.[10] Cleavage of the membrane phospholipids by phospholipase C also encourages fusion by the creation of such lipids.[8] A dramatic change in the force required to deform the membrane must be achieved so that thermal fluctuations are sufficient for their formation. However, a direct measurement of the effect of surface chemistry on the forces required to deform membranes has not been made.

To better understand the molecular mechanisms underlying membrane−membrane interactions, experimen-

† Part of the *Langmuir* special issue entitled The Biomolecular Interface.

‡ Currently at the Department of Chemical Engineering, Carnegie Mellon University, Pittsburgh, PA 15213-3890. E-mail: schneider@cmu.edu.

§ Currently at the School of Chemical Engineering, Purdue University, West Lafayette, IN 47907-1283. E-mail: gl@ecn.purdue.edu.

(1) Cevc, G.; Marsh, D. *Phospholipid Bilayers*: *Physical Principles and Methods*; John Wiley and Sons: New York, 1987.

(2) Israelachvili, J. N.; Wennerström, H. *J. Phys. Chem.* **1992**, *96*, 520−531.

(3) McIntosh, T. J.; Simon, S. A. *Annu. Rev. Biophys. Biomol. Struct.* **1994**, *23*, 27−51.

(4) Chernomordik, L. V.; Melikyan, G. B.; Chizmadzhev, Y. A. *Biochim. Biophys. Acta* **1987**, *906*, 309−352.

(5) White, J. M. *Science* **1992**, *258*, 917−924.

(6) Leckband, D. E.; Helm, C. A.; Israelachvili, J. *Biochemistry* **1993**, *32*, 1127−1140.

(7) Helm, C. A.; Israelachvili, J. N.; McGuiggan, P. M. *Science* **1989**, *246*, 919−922.

(8) Basanez, G.; Goni, F. M.; Alonso, A. *Biochemistry* **1998**, *37*, 3901−3908.

(9) Lindau, M.; Almers, W. *Curr. Opin. Cell Biol.* **1995**, *7*, 509−517.

(10) Chernomordik, L. V. *Chem. Phys. Lipids* **1996**, *81*, 203−213.

10.1021/la026382z CCC: $25.00
Published on Web 01/17/2003

tal work has focused on obtaining distance-resolved intermembrane interaction force data in the form of force curves. The osmotic stress (OS) device, which makes measurements between lipid bilayers in oriented lamellae, has emerged as a powerful technique with high distance and force resolution,[11] making measurements between free bilayers with all membrane fluctuation modes available.[12] However, the limited force range of the OS device has made fusion measurements difficult.

The surface-force apparatus (SFA) makes micronewton force and absolute, angstrom-level separation distance measurements between lipid bilayers supported on rigid mica substrates.[13] SFA measurements between densely packed bilayers show strong steric−hydration forces at short range, with no fusion or strong adhesion even after high degrees of loading. Similar measurements made between depleted bilayers show a long-range attraction between the bilayers followed by a fusion event at high loads.[7,14−16] The attractive forces became more long-ranged and the adhesions stronger as the bilayers were depleted further, leading the authors to ascribe the increased propensity for depleted bilayers to fuse to hydrophobic interactions between exposed lipid tails on each surface. Additionally, bilayers which were phase-separated by the addition of calcium could be made to fuse, presumably due to the exposure of hydrophobic tails at phase boundaries.[6] Because each of these surfaces is chemically inhomogeneous over the large measurement area of the SFA, some uncertainty remains regarding the relationship between hydrophobicity and fusion mechanisms.

The atomic force microscope (AFM) is an experimentally convenient platform for these measurements as the contact area is extremely small (0.01−0.1 μm^2), and gold-coated probes and samples are readily modified by highly stable alkanethiol self-assembled monolayers (SAMs).[17] Used primarily as a surface imaging tool, the AFM has sensitively measured compositionally dependent surface forces,[18] including intersurface van der Waals,[19] electrostatic,[20,21] and hydrophobic[22,23] forces on model surfaces and as a probe of lipid bilayers.[24−30] The fine feature of the pyramidal AFM tip gives this technique superior lateral resolution, allowing for comparison of force data across functional domains. While the AFM makes no absolute measurement of probe−sample separation distance, we have shown that moderately stiff cantilevers ($k \sim 0.5$ N/m) indent Langmuir−Blodgett (LB) bilayers on mica to a constant ultimate depth at high loads, regardless of the composition of the outer monolayer. This provides a reference position to compare multiple force curves.

In this work, we use the AFM to investigate changes in probe chemistry on asymmetric force and adhesion measurements between alkanethiol-SAM-modified tips and LB bilayers. Four films are probed, composed of 18-carbon dialkyl lipids with slightly different monolayer properties and states of headgroup hydration (Figure 1). DSPE (distearoylphosphatidylethanolamine) and DOPE (dioleoylphosphatidylethanolamine) each have a small, poorly hydrated headgroup,[31] and we expect the sugar headgroups of MGDG (monogalactosyldiglyceride) and DGDG (digalactosyldiglyceride) to have much higher degrees of hydration. The DSPE, MGDG, and DGDG monolayers are readily compressed to the liquid-condensed phase (LC), while the DOPE monolayers cannot be compressed beyond the liquid-expanded phase (LE) prior to collapse. The monolayers are deposited onto a monolayer of DSPE on mica, leading to the probe−sample interaction scheme shown in Figure 2.

Apart from the fact that these headgroups represent major constituents of biological membranes, studying this series of molecules allows us to test the effects of changing headgroup hydration state and monolayer phase on the force curves and adhesion measurements. To our knowledge, these are the first AFM measurements made between supported lipid bilayers and hydrophobic probes in water.

Experimental Methods

High-purity DSPE, MGDG, DGDG, and DOPE were purchased from Matreya, Inc. (Pleasant Gap, PA), and used as received. Solutions (0.5 mg/mL) of each lipid were prepared in high-performance liquid chromatography grade chloroform, and equimolar mixtures of lipids were prepared from these stock solutions as necessary. Solutions were stored at room temperature and discarded after 1 month. LB films were deposited onto freshly cleaved mica using a thermostated, computer-controlled LB trough (KSV 5000, KSV Instruments, Helsinki, Finland) which monitors surface pressure (Π) using a Wilhelmy plate. The LB trough was cleaned with a dichromate/sulfuric acid cleaning solution, rinsed thoroughly with Milli-Q-purified water (Millipore, Bedford, MA), and refilled prior to use. Coupons (1 cm^2) of mica were submerged in the water subphase, and 200 μL of the DSPE solution was added dropwise to the water surface. After 5 min, the film was compressed to $\Pi = 25$ mN/m and deposited on the upstroke (5 mm/min). The trough was emptied, rinsed, and refilled with Milli-Q water, and the monolayer of interest was deposited at $\Pi = 25$ mN/m and $\Pi = 5$ mm/min on the downstroke. The bilayer-covered mica coupons were transferred under water to clean beakers.

Oxide-sharpened, pyramidal AFM probes of silicon oxynitride, featuring cantilevers with spring constants (k) ranging from 0.03 to 0.5 N/m, were purchased from Thermomicroscopes (Sunnyvale, CA). Chips were coated in a high-vacuum electron beam thermal evaporator (CVC Products, Inc., Rochester, NY) with 4 nm of chromium and 60 nm of gold, as described previously.[32] Chips were functionalized with hydrophilic and hydrophobic monolayers by ozone cleaning (Jetlight, Irvine, CA) followed by immersion in a ~10 μM ethanolic solution of either mercaptohexadecanol or mercaptohexadecane (courtesy of David Allara) for several hours. The SAMs were periodically characterized by coincubating

(11) Parsegian, V. A.; Rand, R. P.; Fuller, N. L.; Rau, D. C. *Methods Enzymol.* **1986**, *127*, 400−416.
(12) Tsao, Y.; Evans, D. F.; Rand, R. P.; Parsegian, V. A. *Langmuir* **1993**, *9*, 233−241.
(13) Israelachvili, J. N. *Intermolecular and Surface Forces*; Academic Press: New York, 1992.
(14) Horn, R. G. *Biochim. Biophys. Acta* **1984**, *778*, 224−228.
(15) Marra, J. *J. Colloid Interface Sci.* **1985**, *107*, 446−458.
(16) Helm, C. A.; Israelachvili, J. N.; McGuiggan, P. M. *Biochemistry* **1992**, *31*, 1794−1805.
(17) Dubois, L. H.; Nuzzo, R. G. *Annu. Rev. Phys. Chem.* **1992**, *43*, 437−463.
(18) Burnham, N. A.; Dominguez, D. D.; Mowery, R. L.; Colton, R. J. *Phys. Rev. Lett.* **1990**, *64*, 1931−1934.
(19) Butt, H. J. *Biophys. J.* **1991**, *60*, 1438−1444.
(20) Butt, H. J. *Biophys. J.* **1991**, *60*, 777−785.
(21) Ducker, W. A.; Senden, T. J.; Pashley, R. M. *Langmuir* **1992**, *8*, 1831−1836.
(22) Rabinovich, Y. I.; Yoon, R. H. *Langmuir* **1994**, *10*, 1903−1909.
(23) Tsao, Y.; Evans, D. F.; Wennerström, H. *Science* **1993**, *262*, 547−550.
(24) Berger, C. E. H.; Werf, K. O. v. d.; Kooyman, R. P. H.; Grooth, B. G. d.; Greve, J. *Langmuir* **1995**, *11*, 4188−4192.
(25) Ducker, W. A.; Clarke, D. R. *Colloids Surf., A* **1994**, *94*, 275−292.
(26) Dufrêne, Y. F.; Barger, W. R.; Green, J. D.; Lee, G. U. *Langmuir* **1997**, *13*, 4779−4784.
(27) Hui, S. W.; Viswanathan, R.; Zasadzinski, J. A.; Israelachvili, J. N. *Biophys. J.* **1995**, *68*, 171−178.
(28) Zasadzinski, J. A. N.; Helm, C. A.; Longo, M. L.; Weisenhorn, A. L.; Gould, S. A. C.; Hansma, P. K. *Biophys. J.* **1991**, *69*, 755−760.
(29) Zasadzinski, J. A.; Viswanathan, R.; Madsen, L.; Garnaes, J.; Schwartz, D. K. *Science* **1994**, *263*, 1726−1733.
(30) Koleske, D. D.; Barger, W. R.; Lee, G. U.; Colton, R. J. *Mater. Res. Soc. Symp. Proc.* **1997**, *464*, 377−380.
(31) Perera, L.; Essmann, U.; Berkowitz, M. L. *Prog. Colloid Polym. Sci.* **1997**, *103*, 107−115.
(32) Green, J.-B. D.; Lee, G. U. *Langmuir* **2000**, *16*, 4009−4015.

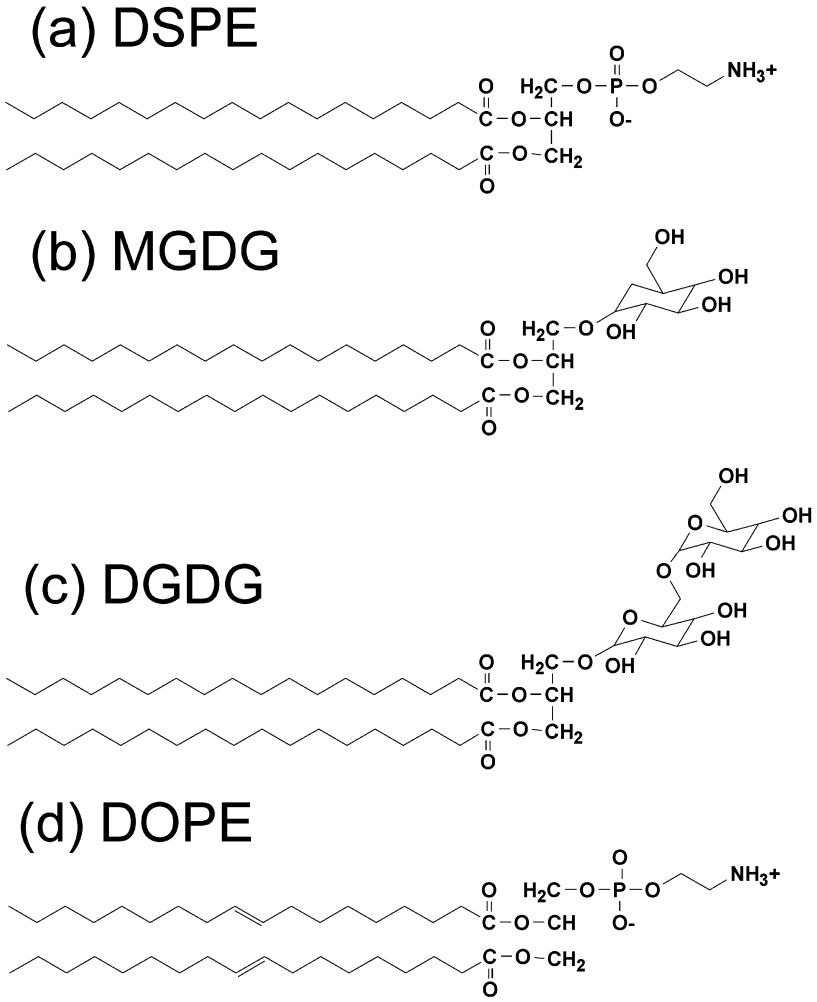

Figure 1. Chemical structures of the lipids studied here. DSPE (a), MGDG (b), and DGDG (c) have fully saturated dialkyl tails, while DOPE (d) has one degree of unsaturation in each tail.

a gold-coated silicon wafer in the same solution as the AFM cantilever chips. The resulting SAMs had wetting properties and changes in ellipsometric parameters similar to literature values.[33] Gold surfaces modified with mercaptohexadecanol ("−OH") had very low contact angles (∼5°), and those modified with mercaptohexadecane ("$-CH_3$") had high contact angles (∼110°). Each chip was rinsed in pure ethanol and water and mounted in a piranha-cleaned fluid cell (Digital Instruments, Santa Barbara, CA) prior to use. To minimize entrapped air bubbles during measurements with hydrophobic tips, the fluid-cell ports were sealed off and the center of the cell was purged with pure water until no bubbles were visible.

Atomic force microscopy images and force measurements were carried out at 25 ± 5 °C using a Multimode Nanoscope IIIa (Digital Instruments, Inc.) with a sample-approach and scanning configuration. A solvent-cleaned, Teflon-coated Viton O-ring (Precision Associates, Minneapolis, MN) was placed onto the mica substrates still immersed in their beakers. Using cleaned stainless steel tweezers, the mica and O-ring were lifted from the beakers and placed onto the AFM scanner capped with a stainless steel sample holder and adhesive (Ted Pella, Redding, CA). The fluid cell was mounted onto the AFM optical-lever "head" and carefully lowered onto the O-ring, sealing it between the cell and substrate. After a wait of an hour for thermal and mechanical equilibration, AFM images were acquired to verify the composition and cleanliness of the surfaces. No changes in the images or force data were observed up to 14 h after deposition, obviating bilayer depletion effects over the time course of this experiment. A 16 × 16 array of force curves, each with 512 data points, was acquired over a 1 μm^2 region that was not previously contacted. A triggering mechanism was employed to initiate retraction after a desired level of loading. Relatively stiff cantilevers (k > 0.3 N/m) were used to minimize cantilever buckling and torsion throughout the measurement of high-load force curves.[34]

After measurements, each microfabricated tip and cantilever was characterized. The radii of curvature (R) were obtained by imaging a $SrTiO_3$ crystal having nanofine sawtooth features with the tip in question.[35] Spring constants (k) were measured by spectral analysis of the detector signal as the cantilever vibrated freely in air, balancing thermal energy with the restoring force of the spring.[36] For springs stiffer than k = 0.5 N/m, spring constants were obtained by measuring a loading curve while pressing the cantilever against a second cantilever of well-calibrated stiffness.[37] The spring constants for cantilevers with similar dimensions did not vary more than 10% from the mean value for each cantilever.

The raw data of detector voltage versus sample piezo voltage were converted to force−displacement curves following standard methods.[21] The extension and retraction of the sample piezo as a function of voltage were independently measured using a capacitance technique, accounting for piezo creep, hysteresis, and nonlinearity.[26] The detector sensitivity (S, in V/nm) was equated to the slope of the detector voltage versus sample position

(33) Bain, C. D.; Troughton, E. B.; Tao, Y. T.; Evall, J.; Whitesides, G. M.; Nuzzo, R. G. *J. Am. Chem. Soc.* **1989**, *111*, 321−335.

(34) Hoh, J. H.; Engel, A. *Langmuir* **1993**, *9*, 3310−3312.

(35) Shieko, S. S.; Moller, M.; Reuvekamp, E. M. C. M.; Zandbergen, H. W. *Phys. Rev. B* **1993**, *48*, 5675−5678.

(36) Walters, D. A.; Cleveland, J. P.; Thomson, N. H.; Hansma, P. K.; Wendman, M. A.; Gurley, G.; Elings, V. *Rev. Sci. Instrum.* **1996**, *67*, 3583.

(37) Tortonese, M.; Kirk, M. *Proc. SPIE-Int. Soc. Opt. Eng.* **1997**, *3009*, 53−60.

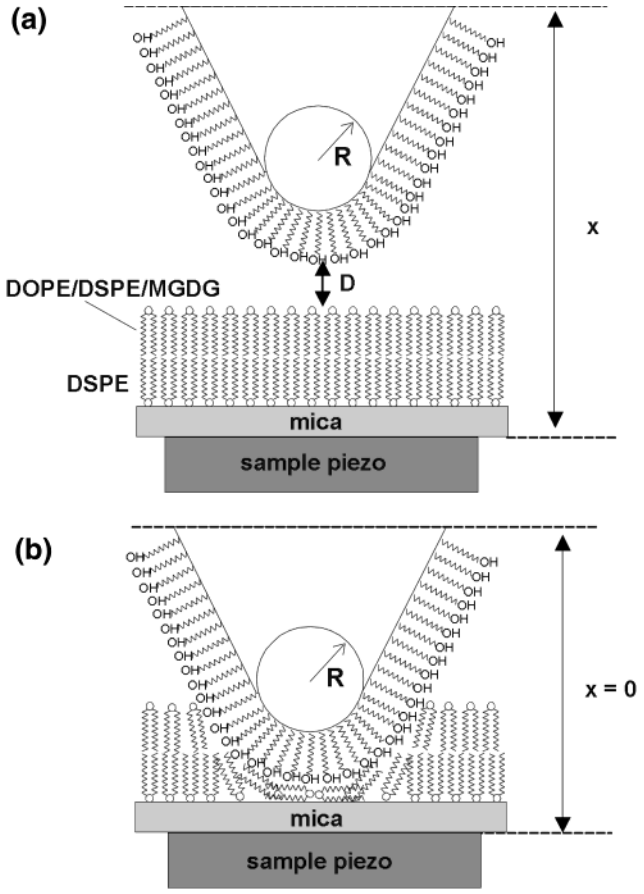

Figure 2. Geometry of the interaction between the alkanethiol-SAM-modified AFM tip and LB bilayers on mica when out of contact (a) and at the point of highest loading (b). The curved shape of the AFM tip apex can be modeled as a sphere of radius R. A monolayer of DSPE, MGDG, DOPE, or a mixture thereof is deposited onto a monolayer of DSPE in the configuration shown. The probe−sample displacement (x) is the distance between the base of the AFM tip and the base of the sample and is a function of the tip−sample separation distance (D) and penetration of the probe into the sample. The probe−sample displacement (x) is set to zero at the point of highest loading (see experimental section).

plot in the constant compliance region (between $F/R = 800$ and $F/R = 1500$ mN/m). This particular regime was selected based on a detailed analysis of force curves with step heights in contact-mode images of mixed monolayers.[38] For the stiff cantilevers used here, S measured on bilayers was consistent with values obtained on rigid samples such as silica. The cantilever deflection (d) was calculated by multiplying the detector voltage by the sensitivity (S). The tip−sample force (F) was calculated by multiplying d by the cantilever spring constant (k), assuming linear spring behavior with the cantilever in its unperturbed, equilibrium position at the beginning of the approach cycle. The force data are scaled by the tip radius of curvature (R) to allow for comparison of multiple data sets.

The AFM does not make an absolute measurement of tip−sample separation distance (D); it measures only relative changes in the tip−sample displacement (x), which we define as the distance between the base of the AFM tip and the base of the substrate (Figure 2a). For reference, we set $x = 0$ at the point of highest loading (Figure 2b). With z defined as above, x is calculated:

$$x = z - d - d_0 \qquad (1)$$

where d_0 is the cantilever deflection at the point of highest loading. Changes in D and deformation effects are both embodied in x.

(38) Schneider, J.; Dufrêne, Y. F.; Barger, W. R.; Lee, G. U. *Biophys. J* **2000**, *79*, 1107−1118.

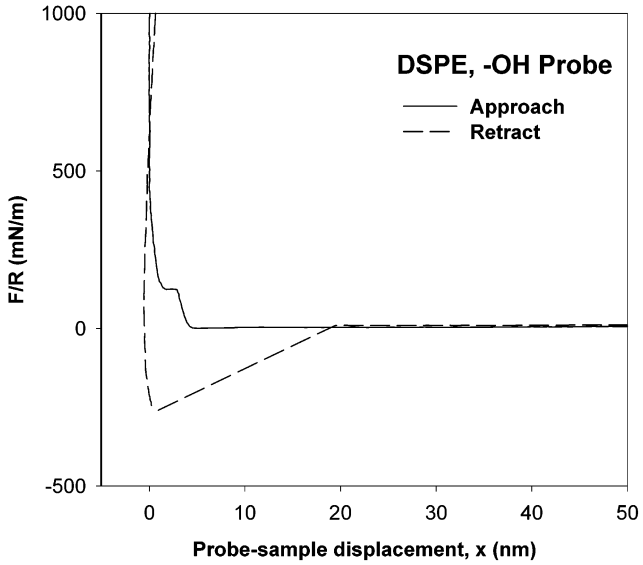

Figure 3. Normalized force (F/R) vs probe−sample displacement (x) curves for the indentation of DSPE/DSPE bilayers using −OH-modified AFM probes. A small jump-in (breakthrough) is observed on approach, and a strong adhesion on retract.

Results

To study the changes in bilayer surface properties with probe chemistry, bilayers of various lipids were deposited onto mica by the LB technique. An LC monolayer of DSPE was transferred onto freshly cleaved mica on the upstroke. A second monolayer of DSPE, MGDG, DGDG, DOPE, or a 1:1 mixture of MGDG and DOPE was transferred onto the DSPE monolayer on the downstroke, yielding a composite bilayer as shown schematically in Figure 2. AFM topography images acquired using unmodified tips show the DSPE, MGDG, and DGDG monolayers transferred onto DSPE monolayers to be very homogeneous, except for a few nanometer scale pinhole defects.[38]

Force measurements between modified tips and LB monolayers were made in Milli-Q water, pH 5.5 ± 0.5, at 25 ± 5 °C on 1 μm^2 regions which had not been previously contacted. Deflection versus sample position plots were converted to force/radius versus displacement plots by the method described in the experimental section. Figure 3 shows a typical approach−retract cycle probing a DSPE/DSPE bilayer using an −OH probe. The force (F) axis is plotted as F/R, where R is the radius of curvature of the tip. Plotting the data in this manner has been shown to remove tip curvature effects for comparison of force and adhesion data using different tips or samples.[13,38] The distance axis (x) is the tip−sample displacement, calculated as described in the experimental section. For the −OH probes, a steeply increasing repulsive force is measured beginning at about $x = 5$ nm. A jump-in is observed at $F/R = 120$ mN/m (all values are averaged for $N = 256$ force curves), followed by a steep repulsion. The jump-in occurs as the probe abruptly penetrates the LB bilayer, and we refer to the force at which it occurs as the "breakthrough force". On retract, the scaled adhesive pull-off force $(F/R)_0 = 300$ mN/m. As reported previously,[26,38] much weaker adhesions ($(F/R)_0 = 1-2$ mN/m) are observed when the probe retraction is initiated before the breakthrough.

The magnitude of the breakthrough force observed using −OH probes is highly dependent on the choice of lipid (Figure 4), and this is likely caused by differences in headgroup chemistry and phase state. For example, the

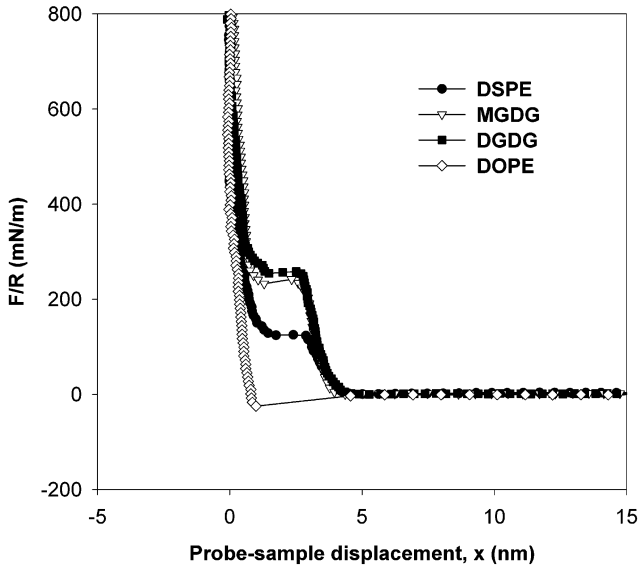

Figure 4. Normalized force (F/R) vs probe−sample displacement (x) curves for the indentation of various LB bilayers using −OH-modified AFM probes (approach only). DSPE/DSPE, MGDG/DSPE, DGDG/DSPE, and DOPE/DSPE bilayers are represented. Lines are to guide the eye.

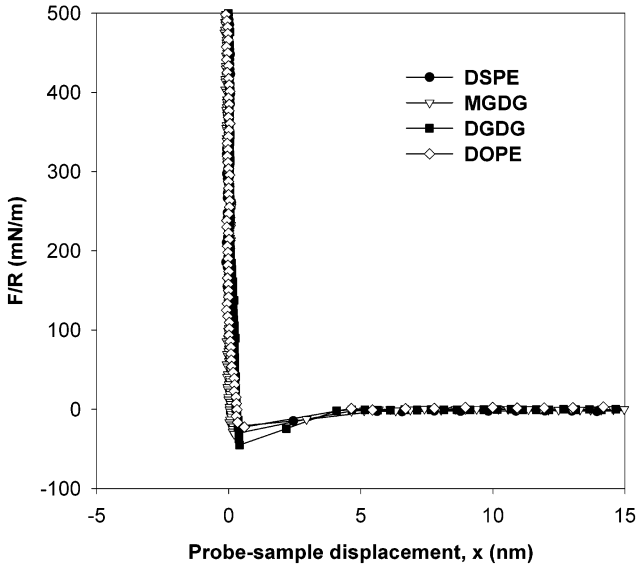

Figure 5. Normalized force (F/R) vs probe−sample displacement (x) curves for the indentation of the LB bilayers of Figure 4 using $-CH_3$-modified AFM probes (approach only). The breakthough event occurs essentially on contact in all cases. Lines are to guide the eye.

MGDG and DGDG lipids have much larger, more highly hydrated headgroups than the DSPE. Unlike the other three, the DOPE monolayer is LE, meaning its compressibility moduli are smaller and the area per lipid is larger. While the molecular-level basis of differences in breakthrough force is somewhat speculative at this point, the differences are statistically significant and repeatable. Generally, lipid monolayers with a large area/molecule and a low area compressibility modulus (DOPE) tend to have lower breakthrough forces. For the more condensed monolayers (DSPE, MGDG, and DGDG), the breakthrough force tends to increase with the hydration state of the headgroups. The larger headgroup of the DGDG does not greatly impact the breakthrough force.

To glean additional information about the membrane interfacial chemistry in fusion processes, we have made

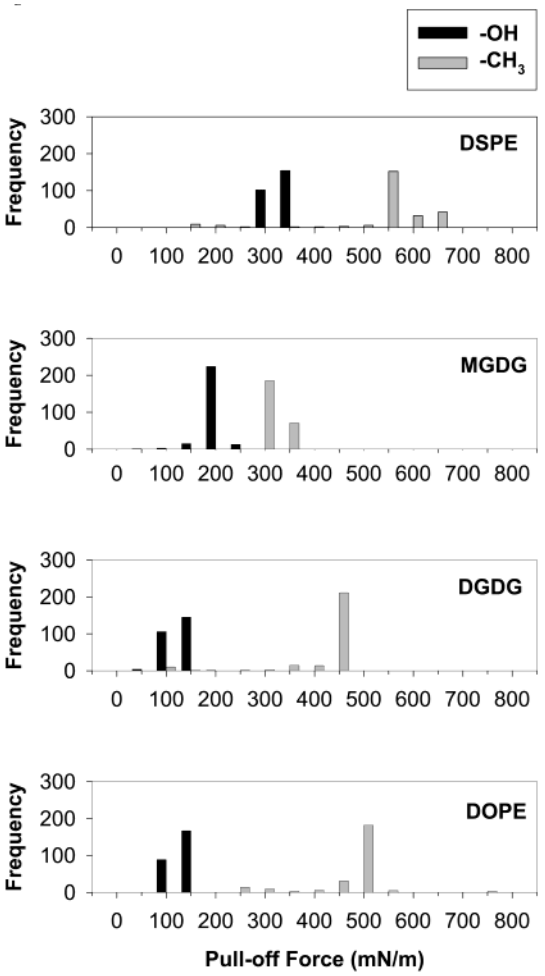

Figure 6. Histograms comparing the normalized pull-off force measured using −OH- and $-CH_3$-modified AFM probes after loading the bilayers to about F/R = 2000 mN/m (postbreakthrough) on approach. The pull-off force is significantly higher when using $-CH_3$ probes in all cases.

similar measurements using hydrophobic ($-CH_3$) probes. In this case, we find very similar behavior across lipid systems as shown in Figure 5. In all cases, the jump-in occurs at $x \sim 5$ nm, essentially just as the probe contacts the bilayer, so the breakthrough force is essentially zero. Pull-off forces are also 2−3 times larger when using the $-CH_3$ probes. The additional barriers provided by the galactolipid headgroups and the LC phase states are all broken down by the presence of the nonpolar $-CH_3$ probe, yielding force curves that are identical to the DOPE curves.

Histograms of the pull-off force and breakthrough force data obtained from the 256 force curves collected over a 1 μm scan size are shown in Figures 6 and 7, respectively. These plots demonstrate the repeatability of our results and establish the significant increase in adhesion and decrease in breakthrough force observed when probing DSPE, MGDG, and DGDG bilayers on DSPE monolayers using $-CH_3$ probes as opposed to −OH probes. Note that the $-CH_3$ probing of DGDG monolayers on DSPE monolayers has several force curves with breakthrough forces above zero, yet still far below the −OH breakthrough force. This phenomenon was observed often with the DGDG monolayers on DSPE monolayers and may be due to more facile tip fouling in the case of DGDG. The higher breakthrough force for the galactolipids compared to DSPE using −OH probes is also demonstrated.

The effects of probe chemistry of lipid bilayer penetration are clearly evident in contact-mode images. Our previous

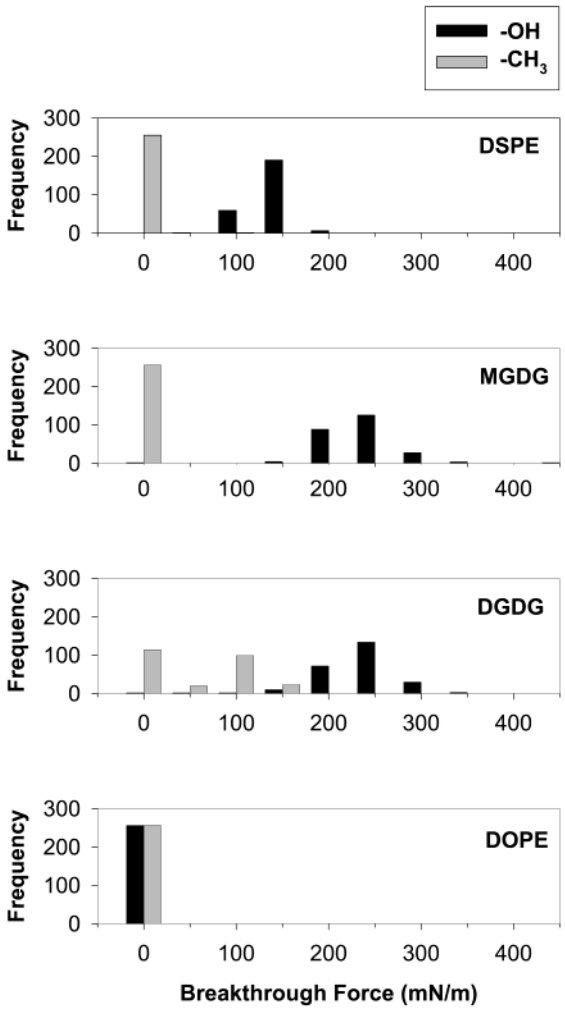

Figure 7. Histograms comparing the normalized brakthrough force measured using −OH- and $-CH_3$-modified AFM probes after loading the bilayers to about F/R = 2000 mN/m on approach. The breakthrough force is reduced to near zero when using $-CH_3$ probes to indent DSPE (a), MGDG (b), and DGDG (c) monolayers deposited onto DSPE monolayers. The breakthrough force is near zero when indenting DOPE (d) monolayers using either probe chemistry.

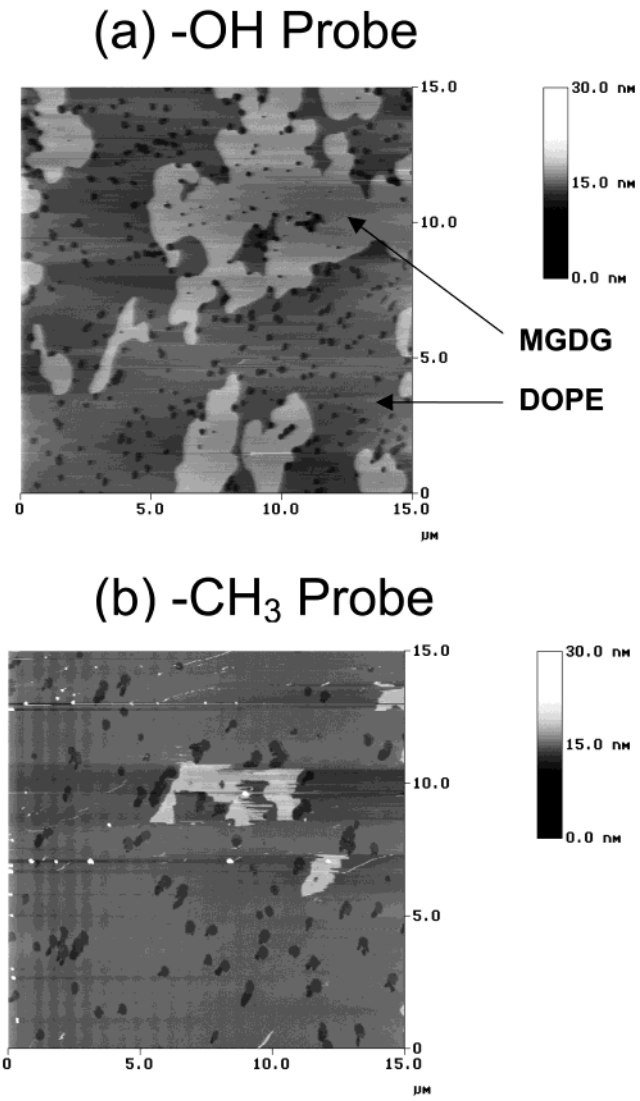

Figure 8. Contact-mode AFM images of a 1:1 mixed monolayer of MGDG and DOPE deposited onto a DSPE monolayer acquired using an −OH probe (a) and a $-CH_3$ probe (b). In both cases, the imaging load is F/R = 20 mN/m, and the scan size 15 μm × 15 μm. The scan rate is 3 Hz in (a) and 10 Hz in (b).

work has outlined the mechanisms for the topography contrast observed in contact-mode images of phase-separated mixed monolayers of DSPE, MGDG, or DGDG and DOPE.[38] At loads below the breakthrough force of DSPE, MGDG, or DGDG, there is a large topographical contrast observed between these LC domains and the LE DOPE owing to a selective breakthrough of the DOPE domains only. Since the breakthrough forces were brought to zero for DSPE, MGDG, and DGDG when using the $-CH_3$ probes, we expect to observe no such topography contrast when imaging mixed monolayers of either of these lipids and DOPE with the same probes, and indeed this is the case.

Figure 8 shows contact-mode AFM images of a 1:1 mixed monolayer of MGDG and DOPE deposited onto a DSPE monolayer using −OH (a) and $-CH_3$ (b) probes, both at an imaging load of 20 mN/m. For −OH probes, the imaging load is below the breakthrough force of MGDG and we observe a large topography contrast between the MGDG and DOPE domains. For $-CH_3$ probes, the contrast is complete as both domains are pierced at the same imaging load. While clean samples show nothing but the pinhole defects (data not shown), an interesting effect occurs when imaging slightly contaminated samples. During imaging, the probe becomes momentarily fouled by the trace contaminant, rendering it more polar and raising the breakthrough force. At this point, the MGDG domains momentarily reappear. Once the probe is clean again, the contrast is removed. Generally, these types of effects were observable only at very high scan rates with some obvious sample contamination, indicating that lipids that may be extracted during force curve measurement or imaging do not significantly modify the probe surface chemistry in these measurements. Still, we did observe a few instances of force curves obtained using $-CH_3$ tips which had features similar to those with −OH probes, which we believe to be a result of tip fouling.

Discussion

The major result we present here is a dramatic change in force curve data when the chemistry of the AFM probe is changed from a hydrophilic probe (−OH) to a hydrophobic probe ($-CH_3$). The general features of the forces curves collected using −OH probes (Figure 4) have been

Table 1. Comparison of Pull-Off Force and Work of Adhesion Data for Different Probe Chemistries[a]

	$(F/R)_0$, −OH (mN/m)	$(F/R)_0$, $-CH_3$ (mN/m)	W, −OH (mJ/m^2)	W, $-CH_3$ (mJ/m^2)	ΔW, −OH/$-CH_3$ (mJ/m^2)	$\Delta(F/R)_0$, −OH/$-CH_3$ (mN/m)	breakthrough force, −OH (mN/m)
DSPE	300	540	64	113	49	154	120
MGDG	180	500	37	105	68	213	210
DGDG	100	420	21	88	67	210	210

[a] The additional attractive forces felt when using the $-CH_3$ probes give rise to the higher sample loading ($\Delta(F/R)_s$), leading to a reduction in the force required to puncture the bilayer.

described in previous reports.[38,39] Briefly, electrostatic forces can be neglected between these charge-neutral surfaces as can forces arising from the suppression of membrane fluctuational modes on approach owing to the anchoring of the bilayers to mica and the bonding of alkanethiol SAMs to gold. Ruling out these forces, we have concluded that the steep repulsion observed on approach represents a combination of mechanical and hydration forces as the AFM probe indents the bilayer at high loads (F/R = 1−100 mN/m). The form of the approach force curves is fitted well by combining the Hertz model for the elastic deformation of a sphere on a flat surface with an exponential expression for the hydration force. At the breakthrough force, the previously elastic response of the bilayer gives way to a plastic deformation of the bilayer, allowing lipids to flow out from underneath the probe as it abruptly penetrates deeper into the sample (Figure 2). After penetration, a second elastic response is observed until the probe rests at a final location within the bilayer. At this point, the stiffness of the sample exceeds the stiffness of the cantilever, and the cantilever can penetrate no further into the bilayer. Using bilayer defects in mixed monolayers of DSPE and DOPE as a reference, we have determined that the probe remains approximately 1.5 nm above the mica surface for the cantilevers used in these studies, meaning that at very large applied loads, the pinhole defects are still observable.

Force curves collected using $-CH_3$ probes have the repulsive steric/hydration barrier completely removed, with only a long-range jump-to-contact observed at x = 5.0 nm. When imaging the DSPE−DOPE mixed monolayer with a $-CH_3$ probe at F/R = 20 mN/m (Figure 8b), we find that the bilayer defects are again about 1.5 nm below the remainder of the image. The onset of the jump-in ($-CH_3$ probes) and the onset of repulsive forces (−OH probes) both occur at x = 5 nm, or 6.5 nm above the bare mica. Space-filling models indicate that DSPE bilayers, as well as composite bilayers of MGDG on DSPE and DGDG on DSPE, have thicknesses between 6.0 and 6.5 nm. We conclude that with either probe chemistry, the probe makes intimate contact with the bilayer surface at very low loads and penetrates to the same final location within the bilayer at high loads (not the bare mica surface).

Still, the major difference between the two probe chemistries is the reduction of the breakthrough force to near zero and the increased pull-off force for $-CH_3$ probes. Interestingly, despite whatever reorganization of the LB layer may be occurring during the force curve measurement, measured adhesion energies compare well with those calculated by interfacial energy considerations alone. Adhesion energies can be calculated from mechanical pull-off forces using the Johnson−Kendall−Roberts (JKR) theory.[40] JKR theory extends the Hertz theory[41] to account for the creation of additional contact area due to adhesive forces. The pull-off force ($(F/R)_0$) is related to the adhesion energy (W) between the probe and sample:

$$W = \frac{2}{3\pi}\left(\frac{F}{R}\right)_0 \tag{2}$$

Values of W calculated by eq 2 are listed in Table 1. Because the JKR theory neglects surface forces outside the contact zone, it is an approximate theory. Muller et al.[42] established a criterion for the applicability of JKR theory based on the parameter μ:

$$\mu = \frac{64}{3\pi}\left[\frac{W^2 R}{4\pi K^2 D_0^3}\right]^{1/3} \tag{3}$$

where D_0 is the surface separation at contact (about 0.1 nm). For the calculated adhesion energies (Table 1), measurements of the radius of curvature (R), and estimates of the composite elastic modulus (K), we calculate μ in the range $50 < \mu < 100$ with JKR theory valid for $\mu > 1$.

Adhesion energies for the $-CH_3$ probes (Table 1) are near 100 mJ/m^2 for the three bilayers. This value agrees well with the theoretical predictions for saturated alkyl chains in water (W = 102 mJ/m^2),[43] implying that any hydrophilic material is excluded from the contact zone after penetration and the bilayer−probe interface can be modeled as contacted layers of hydrocarbon material. Furthermore, because the pull-off force is predicted by thermodynamics, we conclude that mechanical dissipation processes make no significant contribution to the strong adhesion measured. Similar conclusions can be drawn for the −OH probes. AFM adhesion measurements by Sinniah et al.[44] between an −OH SAM and a $-CH_3$ SAM have pull-off forces in the range of F_0 = 1.4 nN, also much smaller than those measured between two $-CH_3$ SAMs (F_0 = 12.5 nN). In this case, resulting adhesion energies also agreed well with those calculated from surface energy considerations.

The differences in surface energy between the −OH and $-CH_3$ probes can also explain the low-load breakthrough of the bilayers using $-CH_3$ probes, and for this we return to JKR theory. For this analysis, we assume that the adhesion energies calculated from the *penetrated* bilayer apply for the entire loading process. JKR theory contends that adhesive forces supply sample loading that augments the external loads. A simple force balance for the force−sample interaction yields

$$F_s = F_c + F_{sf} \tag{4}$$

where F_s is the force exerted by the sample onto the probe, F_c is the load supplied by the deformed cantilever, and F_{sf} is the adhesion-based force driving the probe deeper into the sample to establish a larger contact area. The

(39) Dufrêne, Y. F.; Boland, T.; Schneider, J. W.; Barger, W. R.; Lee, G. U. *Faraday Discuss.* **1998**, *111*, 79−94.
(40) Johnson, K. L.; Kendall, K.; Roberts, A. D. *Proc. R. Soc. London, Ser. A* **1971**, *324*, 301−313.
(41) Hertz, H. *J. Reine Angew. Math.* **1881**, *92*, 156−171.
(42) Muller, V. M.; Yushchenko, V. S.; Derjaguin, B. V. *J. Colloid Interface Sci.* **1980**, *77*, 91−101.
(43) vanOss, C. J. *Colloids Surf., B* **1995**, *5*, 91−110.
(44) Sinniah, S. K.; Steel, A. B.; Miller, C. J.; Reutt-Robey, J. E. *J. Am. Chem. Soc.* **1996**, *118*, 8925−8931.

magnitude of F_{sf} is directly related to the shape of the deformed probe and potential energy gain per unit area created, which is the adhesion energy (W). Approximating the deformed tip shape using Hertz theory, the contact area (A) is

$$A = \pi R\delta \tag{5}$$

where δ is the displacement of the tip into the sample, or $(x_0 - x)$ in terms of our force data. The potential energy brought about by surface forces (U_{sf}) is the product of W and A. The corresponding force is the distance derivative of the potential energy, and we have the following expression for F_{sf}:

$$F_{sf} = \left|\frac{dU_{sf}}{d\delta}\right| = \frac{d(\pi RW\delta)}{d\delta} = \pi RW \tag{6}$$

This is an approximate result, since the Hertz theory (nonadhesive deformation) is used to construct the probe shape. This is the "approximate theory" analysis provided by Johnson et al. in their original presentation of the JKR theory.[40] Since the adhesive forces are much stronger in the $-CH_3$ case, the effective increase in sample load using $-CH_3$ probes rather than $-OH$ probes is given by

$$\frac{\Delta F_s}{R} = \pi\Delta W \tag{7}$$

where ΔW is the increase in W when switching out $-OH$ for $-CH_3$ probes (Table 1). For DSPE/DSPE bilayers, the increase in load is greater than the breakthrough force, and the force required to cause the bilayers to plastically yield can be achieved even with no load supplied by cantilever deflection. For the MGDG and DGDG monolayers on DSPE, the increased load brought about by surface forces is nearly the same as the breakthrough force, allowing for the breakthrough of the bilayers at zero or near zero cantilever deflection. The adhesion-based loading picture appears to be consistent with our observations.

However, these calculations are built upon the assumption that the bilayer/water interfacial energy (γ) is similar to that for a thin layer of alkanes in water (γ = 51 mN/m),[43] while we know the surface of an unperturbed lipid bilayer is much more hydrophilic, with a value somewhere near $\gamma = 20$ mN/m.[13] It is certainly reasonable to expect that the bilayer interfacial energy would increase on loading up to $\gamma = 51$ mN/m as the lipid headgroups separate and more of the bilayer interior is exposed. A more accurate analysis would calculate this change in bilayer interfacial energy with load, probe geometry, and probe chemistry. Due to the molecularity of the confined layer and complications regarding water−surface interactions, a molecular-dynamics simulation would probably be best suited.

We point out that noncontact hydrophobic interactions may cause the bilayer interior to be exposed somewhat before direct contact is made, and in this case the alkane-layer picture could be quite reasonable. Franz and coworkers[45] have presented a model to describe statistical variations in the lipid-bilayer breakthrough force using an activation-volume approach, where the reaction intermediate is a vacancy in the lipid bilayer just below the tip. Since the probability of forming this defect follows Boltzmann statistics, the model predicts a velocity-dependent breakthrough force that was observed by them experimentally. An alternative explanation for our chemistry-dependent behavior is that $-CH_3$ probes stabilize this intermediate, reducing the breakthrough force. In our case, breakthrough forces were zero using $-CH_3$ probes over a wide range of velocities, obviating a similar analysis.

Fusion processes have been directly observed between two bilayers deposited onto mica in the SFA.[6,7,14,16,46] Helm et al.[7] reported hemifusion of cetyltrimethylammonium bromide (CTAB) bilayers at forces near $F/R = 400$ mN/m when the bilayers were first depleted by incubating them in solutions with low concentrations of free CTAB. A significant long-ranged attraction was measured between the depleted bilayers that was not evident for the full bilayers. They ascribed the long-ranged attraction to hydrophobic interactions between the lipid tails exposed in the depleted bilayers and identified a relationship between the long-ranged attraction and a propensity for fusion. There was no perceivable difference between the force curves prior to the fusion event, leading the authors to conclude that repulsive steric/hydration forces are not surpassed by high loading but bypassed by local deformations that join lipid tails from each surface. This hypothesis could not be rigorously tested because of the poor lateral resolution of the SFA and the complex surface chemistry of the depleted bilayer. A relationship between hydrophobic interactions and fusion was also demonstrated between lipid bilayers phase-separated by the addition of calcium, with similar limitations.[6]

The breakthrough event that we observe is a fusion of sorts, in that the lipid bilayer is parted to allow the nanoscopic AFM probe to enter the bilayer, as a small stalk of lipids from one bilayer surface might enter a second bilayer. The $-OH$ probe would be similar to the full bilayer, and the $-CH_3$ probe closer to the depleted bilayer. In both of these studies, a link has been established between hydrophobic surface exposure and ease of fusion. However, our results lead us to a subtly different conclusion: that the effect of the hydrophobic surface is to increase the load on the bilayers while in contact, not to draw hydrophobic material together by out-of-contact attraction or otherwise bypass steric forces.

Of course, neither of these studies represents a completely faithful model of interactions between free bilayers due to the presence of the supporting mica surface. Certainly, hydrophobic surface is exposed in free bilayers by the protrusion of lipids in the stretching of the bilayer during undulations. This work focuses mainly on the contribution of surface chemistry to the free energy of fusion. We argue that the adhesion between exposed lipid tails on opposed bilayers adds a supplemental force that drives their eventual interdigitation.

Conclusions

We have presented AFM force−displacement data for the indentation of a series of lipid bilayers with chemically modified AFM probes. Force curves using hydrophilic probes show an elastic indentation followed by a puncturing of the bilayer at a repeatable, material-dependent breakthrough force. Using hydrophobic probes, these same bilayers are punctured on contact as confirmed by comparison of force curves and imaging of phase-separated bilayers which show a large topographic contrast at low load using $-OH$ probes but none using $-CH_3$ probes.

After breakthrough, the $-CH_3$ probes adhere more strongly to the bilayers than do the $-OH$ probes. Using

(45) Franz, V.; Loi, S.; Müller, H.; Bamberg, E.; Butt, H.-J. *Colloids Surf., B* **2002**, *23*, 191−200.

(46) Marra, J.; Israelachvili, J. *Biochemistry* **1985**, *24*, 4608−4618.

results from the JKR theory, we find that the adhesion can be accounted for in both cases by surface energy considerations, not mechanical effects. The works of adhesion measured for the $-CH_3$ probes compare favorably to independently obtained values for the adhesion of lipid tails in water. Using these adhesion data, a force balance made on the probe−sample interface shows that the load felt by the sample is increased substantially using $-CH_3$ probes rather than −OH probes, reducing the cantilever load required to puncture the bilayer to near zero. These results point to a new mechanism for the fusion of lipid bilayers: an increase in the load felt by contacted hydrophobic regions on either bilayer, forcing them to interdigitate.

Acknowledgment. This work was supported by the Office of Naval Research. J.W.S. was supported by a postdoctoral fellowship from the American Society for Engineering Education. We thank David Allara for providing specialty alkanethiols and John-Bruce Green, Thomas Boland, and Yves Dufrêne for valuable discussions.

LA026382Z